Electrodeposition of manganese dioxide: effect of quaternary amines

A. Biswal[1], B. C. Tripathy[1], T. Subbaiah[1], D. Meyrick[2], M. Minakshi[2]

[1]CSIR—Institute of Minerals and Materials Technology, Bhubaneswar, 751013, Odisha, India

[2]School of Chemical and Mathematical Sciences, Murdoch University, Murdoch, WA, 6150, Australia

Abstract

The effect of quaternary ammonium salts (tetraethyl ammonium bromide, tetrapropyl ammonium bromide, and tetrabutyl ammonium bromide) on the structural, morphological, and electrochemical characteristics of electrolytic manganese dioxide (EMD) obtained from acidic aqueous sulfate solution has been investigated. Physical characterization of the EMD was achieved by X-ray diffraction, scanning electron microscopy, thermogravimetric analysis, differential thermal analysis, and Fourier transform infrared spectroscopy. The charge–discharge profile of the materials was determined to evaluate their potential for alkaline battery applications. The presence of these quaternary ammonium salts as organic additives in the solution increased the current efficiency while decreasing energy consumption during electrochemical deposition of manganese dioxide (MnO_2). All the additives influenced the discharge characteristics of the EMD samples significantly, producing a cathode material with increased cumulative discharge capacity relative to EMD prepared in the absence of additives. This is attributed to the ability of the additives to affect

the particle size and morphology, and therefore electrochemical activity, of electrodeposited materials; the effects in the case of the additives investigated in this work were positive, producing a material with potential application to battery technology.

Keywords: Electrolytic manganese dioxide; Surfactants; Quaternary ammonium salts

Introduction

Natural manganese dioxide (NMD) is a well-researched material that has found wide application in batteries (primary, secondary, and lithium ion) and supercapacitors [1–4]. The recent rapid growth in the type and availability of electronic devices has created demand for batteries with higher capacities. NMD has thus been replaced with synthetic electrolytic manganese dioxide (EMD) of γ-MnO2 form. The salient features of EMD are its low production cost, low environmental impact, high redox potential, high rate capability, better relative performance over a wide temperature range, and long storage life [5–10]. Although γ-MnO2 can be produced by a number of different routes, electrolytically produced γ-MnO2 is the most suitable for battery applications due to its low polarization [11], and it has a niche in the market. EMD can be formed from the direct electrolysis of an aqueous bath of manganese sulfate and sulfuric acid.

The physicochemical and electrochemical properties of EMD are influenced by the composition of the H_2SO_4 electrolyte in the bath. Addition of metal dopant ions to the bath in the electrolytic cell influences the discharge/charge capacity retention of the EMD. Fletcher et al. [12] reported that nickel and titanium dopant ions are beneficial in terms of attaining

excellent rechargeability. Alternatively, addition of organic surfactants to the electrolytic cell appears to be an attractive method as well to improve the electrochemical processes at the substrate/electrolytic solution interface. Surfactants play an important role in modifying the growth pattern (and hence structure) of the electrodeposits through adsorption on the electrode surface. Adsorption of the surfactants not only affects the kinetics of the electron transfer through blocking of active sites but also affects the electrostatic interactions between electroactive species in the electrolytic bath. Consequently, addition of organic surfactants or dopant ions to the electrolytic bath affects the morphology, perhaps crystal structure and mechanical properties of electrochemically deposited material, leading to altered electrochemical behavior of materials.

Surfactants are commonly used in the preparation of various electrode materials by a number of different techniques, such as chemical co-precipitation [13, 14], liquid co-precipitation [15] as well as electrochemical deposition methods [16, 17], and their use has been widely reported in the literature. Ghaemi et al. [17] have reported that electrolytic MnO2 prepared in the laboratory in the absence of surfactant does not have properties appropriate for battery applications. On the other hand, the electrochemical behavior of EMD prepared in the presence of surfactants—namely, t-octyl phenoxy polyethoxyethanol (Triton X-100), cetyltrimethylammonium bromide (CTAB), or sodium n-dodecylbenzenesulfonate (SDBS)—is suitable for battery applications [18]. Among the surfactants studied by Ghaemi et al. [17], Triton X-100 is reported to most improve the charge/discharge cycle behavior of EMD, possibly due to strong adsorption of the surfactant resulting in an increase in charge acceptance capability and current efficiency (CE). The effect of the use of CTAB and SDBS on the performance of Zn–MnO_2 alkaline batteries has also been reported, and the results are equally good [18].

Although dopant metal ions and their effect have been reported [12], to the best of our knowledge no work has been reported on the tetra-alkyl ammonium ions. In this work, quaternary ammonium salts (QAS) as surfactants have been used in the preparation of battery materials. The current work examines the influence of tetraethyl ammonium bromide (TEAB), tetrapropyl ammonium bromide (TPAB), and tetrabutyl ammonium bromide (TBAB) as organic additives. The influence of ammonium salts as cationic surface-active agents on the structural, morphological, and electrochemical characteristics of the EMD produced from acidic aqueous sulfate solutions are investigated. A range of characterization techniques, such as X-ray diffraction, scanning electron microscopy, thermogravimetric and differential thermal analysis, and Fourier transform infrared spectroscopy, and the charge–discharge characteristics were used together to evaluate the possible use of the electrodeposited MnO_2 for alkaline battery applications. This work investigates the suitability of quaternary ammonium salts as organic additives to improve the electrochemical activity of MnO_2 electrode.

Experimental

Materials and methods for producing EMD

Electrolytic manganese dioxide (EMD) was prepared from synthetic aqueous sulfate solutions containing 50 g dm^{-3} $MnSO_4 \cdot 7H_2O$ and 25 g dm^{-3} H_2SO_4 at an anodic current density of 200 A m^{-2} in a glass cell. A schematic diagram of the electrolytic cell arrangement is shown in Fig. 1. Ammonium salts were added at different concentrations into the electrolytic bath during electrolysis. The anodic oxidation of Mn^{2+} to MnO_2 was carried out on a lead (Pb) anode placed in parallel to a stainless steel (SS) cathode. All experiments were carried out at 95 °C for 6 h. The electrodeposited MnO_2 was removed from the anode after

the deposition period and washed thoroughly with deionized water before drying in an oven. The dried mass was ground and sieved through a 100-μm mesh to obtain EMD powder. Subsequently, the resultant product in powder form was washed repeatedly with deionized water until the sample was sulfate free. The EMD powder was finally dried and cooled in a desiccator and subjected to physical and electrochemical characterization.

Structural characterization

X-ray diffractograms were recorded for the EMD powders using PANalytical diffractometer (PW 1830; Philips, Japan) with Mo Kα radiation, $\lambda = 0.71073$ Å. The scans were recorded in 2θ range 5–45°. Fourier transform infrared (FT-IR) spectrographs were recorded on a Nicolet 6070 spectrophotometer in the frequency range 400–4,500 cm^{-1}. A scanning electron microscope (SEM) (JEOL JSM 6510, Japan) was used to examine the surface morphology of the EMD samples.

Thermal analysis

Differential thermal analysis (DTA) and thermogravimetry (TG) (Perkin Elmer Diamond) was carried out under inert atmosphere over a temperature range between 30 and 1,000 °C with a heating rate of 5 °C min^{-1}.

Electrochemical characterization

A suspended cell arrangement was employed for evaluating the electrochemical behavior of the prepared EMD samples. The discharge profile was recorded at room temperature

(27 ± 2 °C) while imposing constant discharge and charge currents in 9 M KOH electrolyte solution. A schematic diagram of the electrolytic cell arrangement for charge–discharge study is given in Fig. 2. The experimental cell consisted of a zinc strip (100 × 10 mm) as anode and EMD cathode. The cathode was prepared from a uniform mixture of EMD and graphite powder with polyvinyl alcohol (PVA) as binder. The mixture was placed in a stainless steel mesh to facilitate electrical contact, placed in a die, and then subjected to a pressure of 9,800 kPa by means of a pressure die machine. The resulting EMD was positioned in the cell assembly and allowed to equilibrate for 1 h at its open circuit potential before commencing the electrochemical processes. The applied discharge current was 1 mA with a cut-off voltage (COV) of 0.9 V. The applied charge current was 2 mA with a cut-off voltage of 1.8 V. The discharge capacities were recorded for up to 14 cycles. The galvanostatic measurements were carried out using a BITRODE deep cycle battery tester (LCN1-25-24, USA).

Results and discussion

Electrolysis

The electrochemical parameters (current efficiency, CE, and energy consumption, EC) of electrodeposited EMD prepared in the presence of QAS additives tetraethyl ammonium bromide (TEAB), tetrapropyl ammonium bromide (TPAB), and tetrabutyl ammonium bromide (TBAB) are given in Table 1.

In the absence of additive in the bath, CE of 91.4 % was observed and with the introduction of a small amount of additive (TEAB) the CE increased to 99.1 %, while the EC decreased

from 1.68 to 1.56 kWh kg^{-1} during electrolysis. This suggests strong adsorption of the additives on the electrode surface as reported by Ghaemi et al. [17].

In general, the electrodeposition of manganese dioxide from an acidic sulfate solution proceeds through the following reactions:

At Anode: $Mn2{+}{+}2H2O \rightarrow MnO2+4H{+}{+}2e-$ (1)

At Cathode: $2H{+}{+}2e- \rightarrow H2$ (2)

At the anode, the formation of MnO_2 does not take place in a single step; rather, Mn^{3+} as an intermediate species is first formed [19, 20] together with some solid intermediates such as MnOOH(s) and Mn_2O_3(s). The Mn^{3+} ion, being unstable in hot acidic solution, undergoes a disproportionation reaction forming Mn^{4+} and Mn^{2+}.

$Mn2{+}sol \rightarrow Mn3{+}ads+e-$ (3)

$2Mn3{+}ads \rightarrow Mn4{+}ads+Mn2{+}sol$ (4)

The Mn^{4+} is converted to solid MnO_2 through a hydrolysis reaction with fast kinetics [21, 22], while Mn^{2+} ions remain in solution. During the electrodeposition process Mn^{3+} ions may be trapped in the MnO_2 lattice, possibly resulting in defects in the crystal structure.

Adsorption of surfactants at the substrate/electrolytic solution interface may inhibit the rate of Eq. (3) due to the blocking of the active growth sites, thereby allowing electrodeposition preferentially on the crevices [23]. The electron/ion transfer kinetics mostly depend on the degree of coverage of the electrode due to either mechanical blocking or through electrostatic interactions [24, 25]. This could change the electrical double layer characteristics and thus

affect the interfacial energy, dielectric constant, potential, and current distribution at the electrodes resulting in modified crystal growth. Hence, the organic surfactants play a vital role in facilitating the formation of compact deposits with greater surface area. However, careful monitoring of appropriate surfactant concentration during electrolysis is required to achieve reproducibility. Higher concentrations may lead to irregular morphology owing to higher ohmic potential drop and electrode overvoltage [26–28].

X-ray diffraction analysis

The most common forms of MnO_2 (γ-, ε-, and β-MnO_2) are related to the mineral structures ramsdellite, akhtenskite, and pyrolusite with orthorhombic, hexagonal, and tetragonal modifications of MnO_2, respectively. The **γ**- and ε-forms are electrochemically active [29].

In the present study, all the electrodeposited MnO_2 samples were subjected to X-ray diffraction (XRD) analyses. XRD profiles of EMD samples produced in this work (Fig. 3) were consistent with hexagonal γ-MnO_2 having lattice parameters $a = 6.36$ Å, $b = 10.15$ Å, and $c = 4.09$ Å (ICDD-JCPDS No. 14-0644) [30, 31]. The XRD pattern for the sample prepared in the absence of additive yielded diffractive peaks assigned to the (120), (131), (300), (160), and (421) planes. Addition of as much as 50 ppm organic additive (TEAB, TPAB, and TBAB) did not affect the crystal structure and pattern (Fig. 3b–d) of the produced EMD materials. Similarly, lower quantities of additives (~10 ppm) did not produce changes in crystal structure or reflections (Fig. 3b–d, shown for comparison), suggesting that the quantity of additives does not modify the structure. Note that the broad diffraction peaks in the patterns indicate that crystallite size within the EMD samples is within a range suitable

for exploitation of the material for high power applications [31]. A very narrow diffraction peak indicates larger particle sizes, which may not be suitable for rechargeable battery applications due to lower surface area.

FTIR analysis

FT-IR spectroscopy, being an important tool for detecting the presence of hydroxyl ions and water molecules in the specimen, was employed for analysis of the EMD material (Fig. 4). The presence of OH^- groups and water molecules associated as bound water within the crystal structure can influence the electrochemical activity of the EMD [32–34]. For the sake of simplicity, the EMD sample prepared in the presence of 50 ppm organic additive was selected for all physical characterization (other than XRD, by which all samples were analyzed). The broad absorption band detected in the region 400–600 cm^{-1} confirms the formation of γ-MnO_2 [35]. The absorption band at 1,100 cm^{-1} can be attributed to the MnO_2 stretching mode and/or O–H bending vibrations [35] associated with hydrogen bonding, indicating the presence of bound water molecules [32, 33]. The strong absorption band at ~1,630 cm^{-1} can be attributed to O–H bending vibrations associated with the water of crystallization [32] and a broad absorption band at ~3,400 cm^{-1} is due to O–H stretching vibrations [32–34]. A weak absorption band is observed at ~1,400 cm^{-1} indicating O–H stretching vibrations [36].

Surface morphology

Changes in deposit morphology may influence the current efficiency, stability, and rechargeability of EMD [17]. Surfactants have a significant effect on the deposit pattern due

to their control on nucleation and growth mechanisms during electrodeposition [37], as well as various interactions with the species present in the electrolytic solutions [38]. The presence of the QAS additives in the electrolysis bath influenced the EMD particle size (Fig. 5). Discrete particles with no agglomeration and small grain size are observed in the case of 50 ppm TEAB and TPAB added (Fig. 5b–c), while a larger grain size is observed for EMD deposited in the absence of additives (Fig. 5a). This suggests that the organic additives have promoted nucleation and current distribution during electrodeposition, resulting in the observed increase in current efficiencies (CE) of the EMD samples (Table 1) and the associated decrease in power consumption during electrodeposition in all cases. However, for EMD electrodeposited in the presence of TBAB, a larger particle size distribution was observed (Fig. 5d). This is also reflected in the measured BET surface area of the samples. The EMD samples with TEAB and TPAB at 50 mg dm^{-3} showed the highest BET surface areas of ~87.2 and 79.6 m^2g^{-1}, respectively, whereas TBAB at the same concentration showed a measured surface area of 63 m^2 g^{-1}. Well-dispersed EMD particles with rough surfaces and pores (i.e., high surface area) have superior contact with the graphite (in electrode construction) and electrolyte, facilitating better cyclic reversibility of the synthesized product.

Thermal analysis

Thermogravimetric analysis of the EMD samples in the absence and presence of the organic additives was performed (Fig. 6). The mass loss up to 110 °C is likely due to the removal of physically adsorbed water molecules, while that in the range 110 to 300 °C may be attributed to the removal of chemically bound water present in the EMD samples (Fig. 6). It is clearly evident that there have been weight losses in the temperature regions 400–600 and 600–

900 °C, which may be attributed to the formation of lower valence oxides of manganese, Mn_2O_3 and Mn_3O_4, during thermal decomposition of EMD samples [32, 39, 40]. In any case, the organic additives TEAB, TPAB, and TBAB have virtually no effect on the thermogravimetric behavior of the synthesized EMD.

The responses of the EMD samples to differential thermal analysis (DTA) can be seen in Fig. 7. Sharp endo peaks at ~100 °C and broad endo peaks at ~300 °C can be seen, indicating the removal of adsorbed and chemically bound crystalline water, respectively. The two endo peaks at ~500 °C and ~900 °C again may correspond to the formation of lower valence oxides of manganese, Mn_2O_3 and Mn_3O_4, during thermal decomposition of the EMD samples. The nature of the thermograms was not affected by the presence of the organic additives.

Electrochemical activity

The electrochemical behavior of the EMD samples was characterized by galvanostatic experiments. The charge and discharge characteristics enable evaluation of the suitability of the prepared EMD as a battery material. The EMD samples prepared in the absence and presence of organic additives were subject to charge–discharge reactions in 9 M potassium hydroxide aqueous solutions. The reactions at cathode and anode are as follows:

Cathode: $MnO2+H2O+e-\rightleftarrows MnOOH+OH-$

Anode: $Zn+2OH-\rightleftarrows ZnO+H2O+2e-$

NetReaction: $Zn+2MnO2+H2O\rightleftarrows ZnO+2MnOOH$

The electron discharge from manganese dioxide is thought to proceed via a homogeneous reversible reaction by the movement of protons and electrons into the lattice, resulting in a gradually decreasing value of x in MnO_x, from $x = 2.0$ to 1.5 [41–43]. This mechanism is attributed to the reversible conversion of MnO_2 into MnOOH in the solid phase. The second electron discharge of MnO_2, which proceeds either in solid or in solution phase, leads to the formation of $Mn(OH)_2$, a product formed during recharging of γ-MnO_2 [34]. The typical discharge characteristics of the pellets made from EMD powders prepared from aqueous sulfate solutions in the absence and presence of organic additives TEAB, TPAB, and TBAB are shown in Figs. 8, 9, 10, and 11. The discharge capacity of 240 mAh g^{-1} (870 C g^{-1}) was obtained from the EMD containing no additives, against 160 mAh g^{-1} (580 C g^{-1}) for the reported values for EMD in the absence of additives [30]. It is very interesting to note that the addition of organic additives to the electrolytic cell during electrodeposition of MnO_2 produced a significant effect on the discharge performance of the EMD. Addition of TEAB increased the discharge capacity to 298 mAh g^{-1} (closer to the theoretical value of 308 mAh g^{-1} for the $1e^-$ process [42, 44]). The EMD prepared in the presence of the other additives (TPAB and TBAB), in the electrolytic solutions at concentrations of 50 ppm, showed discharge capacities of 278 and 275 mAh g^{-1}, respectively. It is also interesting to note that the discharge capacity of the EMD prepared in the absence of additive fades rapidly (Fig. 8a). However, EMD prepared in the presence of organic additives was able to maintain discharge capacity over a greater number of cycles (Fig. 8b–d).

Addition of 5 ppm and 10 ppm TEAB (Fig. 9b–c) increased the initial discharge capacity to 285 and 290 mAh g^{-1}, respectively, from approximately 245 mAh g^{-1} for the EMD prepared with no additives present. A further increase in the concentration of TEAB to 50 ppm (Fig. 9e) increased the discharge capacity to a maximum of 298 mAh g^{-1} (closer to the

theoretical value of 308 mAh g^{-1} for the $1e^-$ process [42, 44]). However, further increasing the concentration of TEAB to 100 ppm (Fig. 9d) caused a lowering of the discharge capacity to 234 mAh g^{-1}. A similar behavior was observed for both 10 ppm of TPAB (Fig. 10b) and TBAB (Fig. 11b), where initial discharge capacities of 259 and 251 mAh g^{-1} were obtained. The EMD prepared in the presence of these additives in the electrolytic solution at concentrations of 50 ppm (TPAB and TBAB) showed initial discharge capacities of 278 and 275 mAh g^{-1}, respectively, while again a concentration of 100 ppm for these additives decreased the discharge capacities, in these cases to 252 and 233 mAh g^{-1} for TPAB and TBAB, respectively. A similar trend was reported by Ghaemi et al. [17], although the discharge capacities were approximately half those observed in this study. The lower discharge capacity obtained for EMD electrodeposited in the presence of TBAB may be due to the sterically bulky butyl groups of the TBAB, which may block the active sites of the anode, therefore producing larger crystallites.

The data obtained in this study suggest that the use of TEAB and TPAB during the electrodeposition of manganese dioxide is beneficial in terms of cycle stability and discharge capacity.

Conclusions

The presence of quaternary ammonium salts (TEAB, TPAB, and TBAB) as organic additives during the electrodeposition of MnO_2 (to produce EMD) has not affected the crystal pattern of the synthesized EMD samples; all the samples show the characteristics of γ-MnO_2 form. This is confirmed by the presence of a broad absorption band in the infrared region 400–

600 cm^{-1}. Although the presence of organic additives does not show any significant effect on the TG and DTA behavior of the EMD samples, formation of lower valence manganese oxides such as Mn_2O_3 and Mn_3O_4 at higher temperatures was evident, as is the case for EMD prepared from solutions free of additives. The presence of these organic additives during electrodeposition of MnO_2 resulted in an increase in current efficiencies of the EMD material and decreased the energy consumption of the electrodeposition cell. The presence of TEAB and TPAB resulted in well-dispersed small particles yielding, in turn, a high BET surface area of ~87.2 and 79.6 m^2g^{-1}, respectively. The presence of these organic additives influenced the discharge performance of the EMD significantly by increasing the discharge capacities of the material from ~240 mAh g^{-1} (870 Cg^{-1}) for EMD prepared without additives to ~290 mAh g^{-1} (1,050 Cg^{-1}) for EMD prepared in the presence of TEAB and TPAB, and ~275 mAh g^{-1} (995 Cg^{-1}) in the presence of TBAB. The electrochemical properties of EMD were enhanced by the presence of QAS during electrodeposition, and the material produced by these methods has potential for battery applications.

Acknowledgments

The author (M. M.) wishes to acknowledge the Australian Research Council (ARC). A part of this work was supported under Australian Research Council (ARC) Discovery Project funding scheme (DP1092543).

References

1. Yao YF, Gupta N, Wroblowa HS (1987) J Electroanal Chem Interfacial Electrochem 223:107–117
2. Dell RM (2000) Solid State Ionics 134:139–158
3. Adelkhani H, Ghaemi M (2008) Solid State Ionics 179:2278–2283
4. Tu J, Zhao XB, Xie J, Cao GS, Zhuang DG, Zhu TJ, Tu JP (2007) J Alloy Compd 432:313–317
5. Urfer A, Lawrance GA, Swinkels DAJ (1997) J Appl Electrochem 27:667–672
6. Kordesch KV, Dekker M (1974) Batteries. Dekker, New York
7. Kordesch KV, Welssenbacher M (1994) J Power Sources 51:61–78
8. Machefaux E, Hill LI, Guyomard D. The Electrochemical Society, 204th Meeting, Abstract 365
9. Jantscher W, Binder L, Fiedler DA, Andreaus R, Kordesch K (1999) J Power Sources 79:9–18
10. Chou S, Cheng F, Chen J (2006) J Power Sources 162:727–734
11. Nartey VK, Binder L, Huber A (2000) J Power Sources 87:205–211
12. Fletcher S, Galea J, Hamilton JA, Tran T, Woods R (1986) J Electrochem Soc 133:1277–1281
13. Li Y, Xie HQ, Wang JF, Chen LF (2011) Mater Lett C5:403
14. Jiang RR, Huang T, Liun JL, Zhuang JH, Yu AS (2009) Electrochim Acta 54:3047–3052
15. Zhang H, Wang Y, Liu C, Jiangm H (2012) J Alloy Compd 517:1–8
16. Zhao T, Jiang H, Ma J (2011) J Power Sources 196:860–864
17. Ghaemi M, Fard LK, Neshati J (2005) J Power Sources 141:340–350
18. Ghavami RK, Rafiei Z, Tabatabai SM (2007) J Power Sources 164:934–946
19. Nijjer S, Thonstad J, Haarberg GM (2000) Electrochim Acta 46:395–399
20. Kao WH, Weibel VJ (1992) J Appl Electrochem 22:21–27
21. Prelot B, Poinsignon C, Thomas F, Schouller E, Villieras F (2003) J Colloid Interface Sci 257:77–84
22. Prelot B, Villieras F, Pelletier M, Razafitianamaharavo A, Thomas F, Poinsignon C (2003) J Colloid Interface Sci 264:343–353
23. Boto K (1975) Electrodeposition Surf Treat 3:77–95
24. Kozarac Z, Nikolic S, Ruzic I, Cosovic B (1982) J Electroanal Chem 137:279–292
25. Felhosi I, Telegdi J, Palinkas G, Kalman E (2002) Electrochim Acta 47:2335–2340
26. Wen DS, Wang BX (2002) Int J Heat Mass Transfer 45:1739–1747
27. Mobarak AA, Hassan MSM, Sedahmed GH (2000) J Appl Electrochem 30:1269–1276
28. Rusling JF, Wang Z, Owlia A (1990) Colloid Surf 48:173–184
29. Bodoardo S, Penazzi N, Spinelli P, Arrabito M (2001) J Power Sources 94:194–200
30. Thackeray MM (1997) Prog Solid State Chem 25:1–71
31. Kurimoto H, Suzuoka K, Murakami T, Xia Y, Nakamura H, Yoshio M (1995) J Electrochem Soc 142:2156–2162
32. Fernandes JB, Desai BD, Dalal VNK (1983) Electrochim Acta 28:309–315
33. Ananth MV, Pethkar S, Dakshinamuthi K (1998) J Power Sources 75:278–282
34. Ruetschi P (1984) J Electrochem Soc 131:2737–2744
35. Abbas H, Nasser SA (1996) J Power Sources 58:15–21
36. Fitzpatrick J, Maclean LAH, Swinkels DAJ, Tye FL (1997) J Applied Electrochem 27:243–253
37. Besenhard JO, Gurtler J, Komenda P, Paxions A (1987) J Power Sources 20:253–258
38. Khimyak YZ, Klinowski J (2000) J Mater Chem 10:1847–1855
39. Brenet JP, Faber P (1995) Symp I.S.E. Batteries, Marcoussis, France
40. Sharp JH, Tinsley DM (1971) J Therm Anal 3:43–48
41. Ghaemi M, Biglari Z, Binder L (2001) J Power Sources 102:29–34
42. Minakshi M (2008) J Electroanal Chem 616:99–106
43. Minakshi M, Singh P, Carter M, Prince K (2008) Electrochem Solid State Lett 11:A145
44. Kordesch K, Gsellmann J, Peri M, Tomantschger K, Chemelli R (1981) Electrochim Acta 26:1495–1504

Fig. 1 Schematic diagram of electrolytic cell arrangement for depositing electrolytic manganese dioxide (EMD)

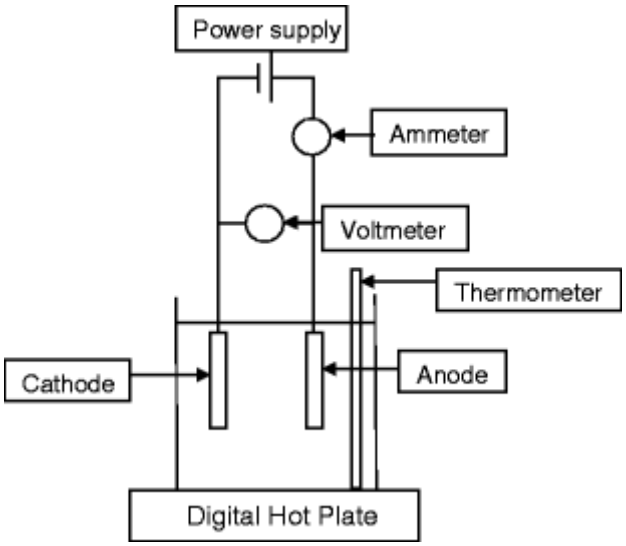

Fig. 2 Schematic diagram of electrolytic cell arrangement for galvanostatic measurements (charge–discharge) of electrolytic manganese dioxide (EMD)

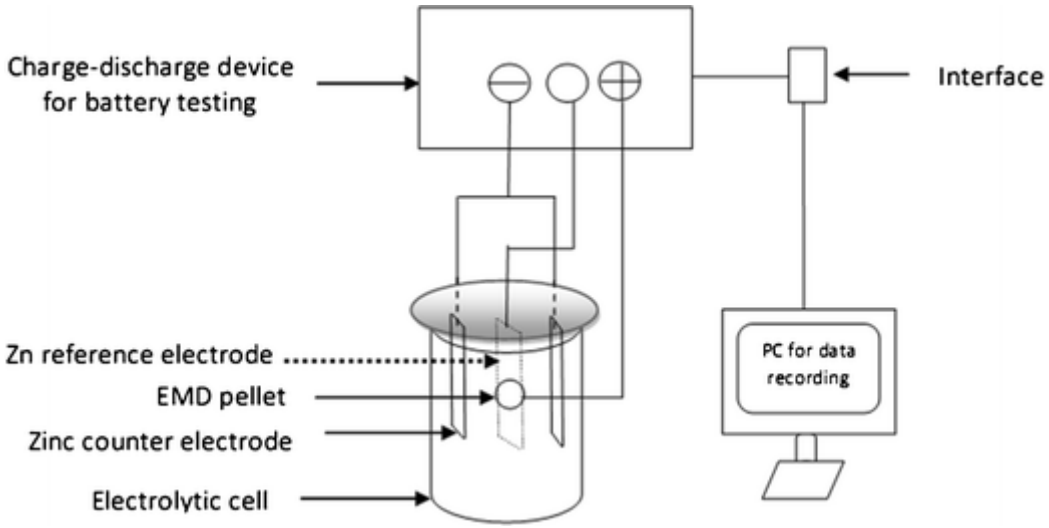

Fig. 3 X-ray diffraction patterns of EMD on the lead substrate from a bath (**a**) free of additives and containing various organic additives: **b** 50 ppm TEAB, **c** 50 ppm TPAB, **d** 50 ppm TBAB, **e** 10 ppm TEAB, and **f** 10 ppm TPAB

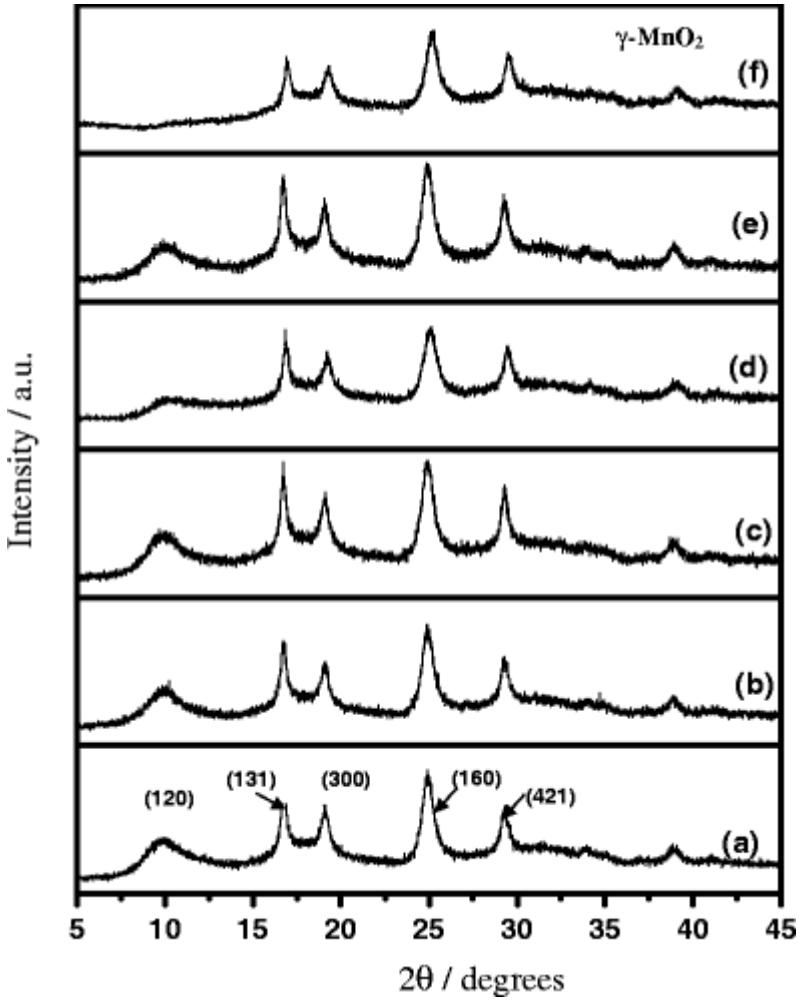

Fig. 4 FTIR spectra of EMD samples prepared in a bath (**a**) free of additives and containing various organic additives: **b** 50 ppm TEAB, **c** 50 ppm TPAB, **d** 50 ppm TBAB

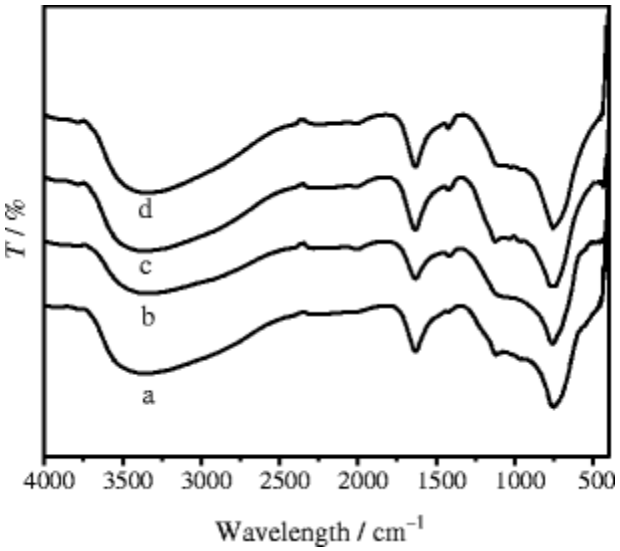

Fig. 5 SEM images of EMD samples prepared from a bath (**a**) free of additives and containing various organic additives: **b** 50 ppm TEAB, **c** 50 ppm TPAB, and **d** 50 ppm TBAB

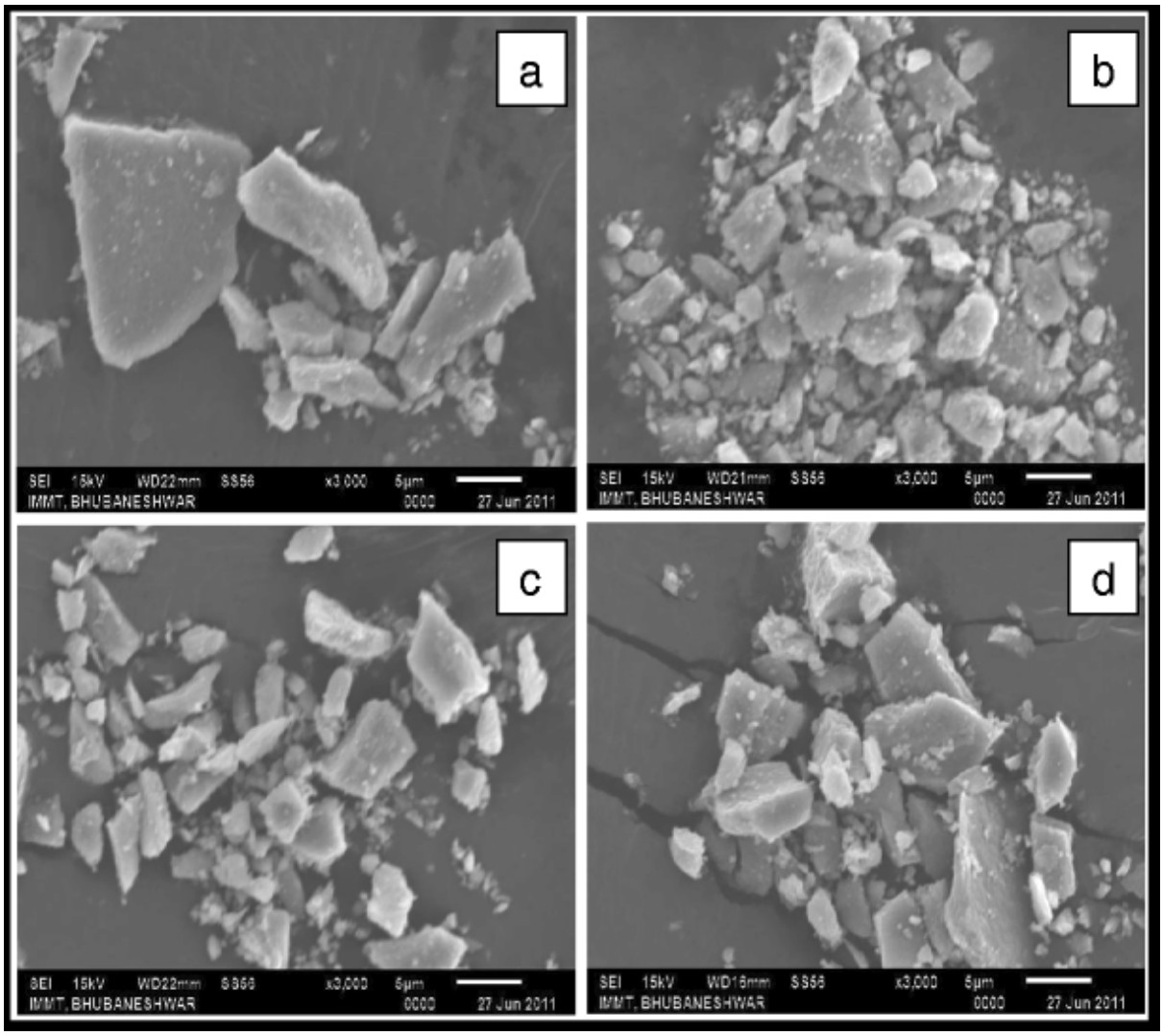

Fig. 6 Thermogravimetric analyses of EMD samples prepared from a bath (**a**) free of additives and containing various organic additives: **b** 50 ppm TEAB, **c** 50 ppm TPAB, and **d** 50 ppm TBAB

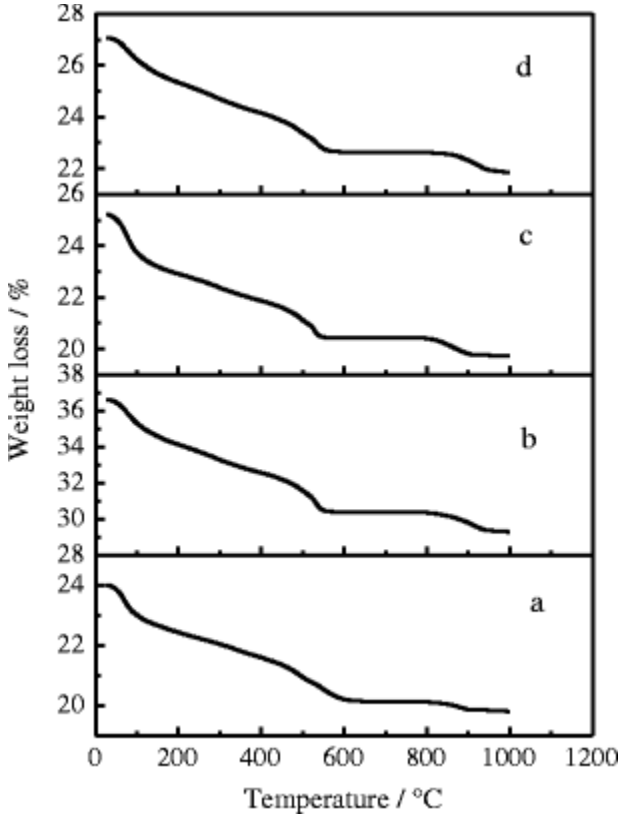

Fig. 7 Differential thermal analyses of EMD samples prepared from a bath (**a**) free of additives and containing various organic additives: **b** 50 ppm TEAB, **c** 50 ppm TPAB, and **d** 50 ppm TBAB

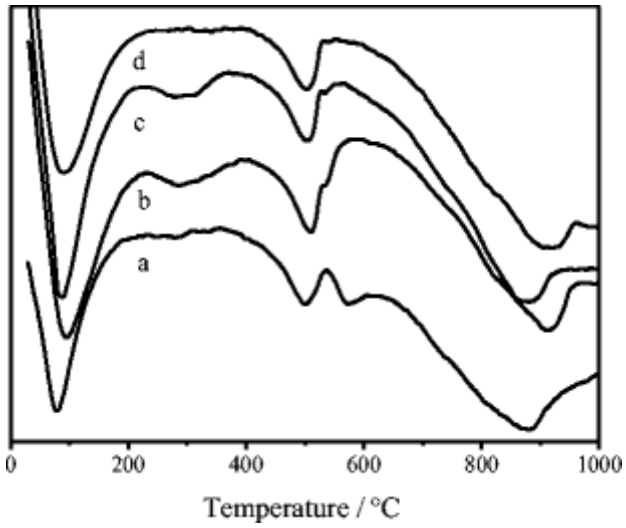

Fig. 8 Discharge and specific capacities versus cycling behavior of EMD samples prepared from an electrolytic bath (**a**) free of organic additives and containing **b** 50 ppm TBAB, **c** 50 ppm TPAB, and **d** 50 ppm TEAB

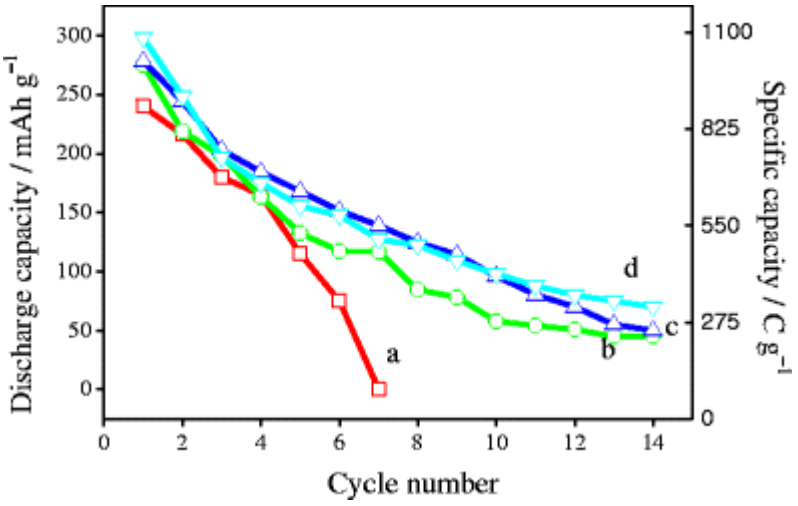

Fig. 9 Discharge and specific capacities versus cycling behavior of EMD samples prepared from a bath containing TEAB in different concentrations. **a** 0, **b** 5, **c** 10, **d** 100, and **e** 50 ppm

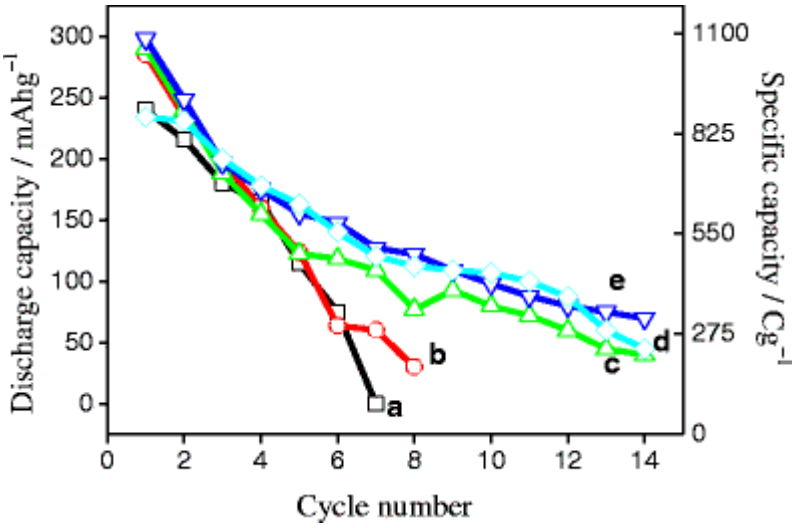

Fig. 10 Discharge and specific capacities versus cycling behavior of EMD samples prepared from a bath containing TPAB in different concentrations. **a** 0, **b** 10, **c** 100, and **d** 50 ppm

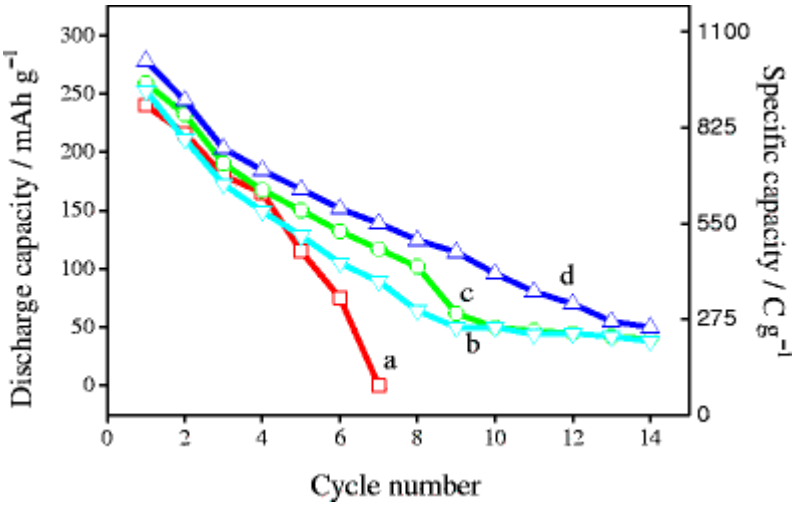

Fig. 11 Discharge and specific capacities versus cycling behavior of EMD samples prepared from a bath containing TBAB in different concentrations. **a** 0, **b** 10, **c** 100, and **d** 50 ppm

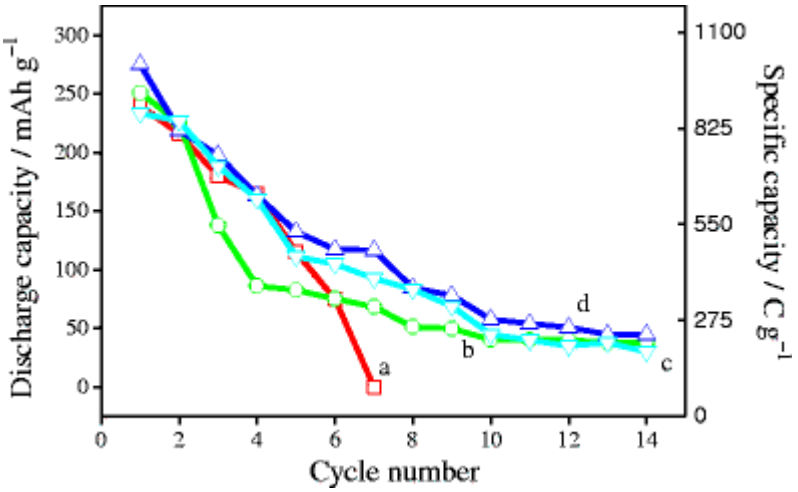

Table 1 Effect of additives on the electrodeposition characteristics of electrolytic manganese dioxide (EMD)

Additive	**Additive (mg dm^{-3})**	**CE (%)**	**EC (kWh kg^{-1})**	**BET surface area (m^{2}g^{-1})**	**Particle size (d_{50}) (µm)**
Blank	0	91.4	1.68	55.82	84.45
TEAB	10	99.1	1.56	81.4	37.72
	50	98.2	1.59	87.23	35.62
	100	95.5	1.63	ND	58.86
TPAB	10	99.2	1.55	82.57	50.48
	50	97	1.58	79.67	48.38
	100	95.1	1.64	ND	80.65
TBAB	10	99.5	1.5	68.81	75.94
	50	96.5	1.58	63.01	70.63
	100	94.1	1.59	ND	66.11